



Research paper

Irradiation by γ -rays reduces the level of H3S10 phosphorylation and weakens the G2 phase-dependent interaction between H3S10 phosphorylation and γ H2AX



Eva Bártová ^{a,*}, Gabriela Lochmanová ^{b,1}, Soňa Legartová ^a, Jana Suchánková ^a, Radek Fedr ^a, Jana Krejčí ^a, Zbyněk Zdráhal ^{b,c}

^a Institute of Biophysics of the Czech Academy of Sciences, Královopolská 135, 612 65, Brno, Czech Republic

^b Central European Institute of Technology (CEITEC), Kamenice 753/5, 625 00, Brno, Czech Republic

^c National Centre for Biomolecular Research, Kamenice 753/5, 625 00, Brno, Czech Republic

ARTICLE INFO

Article history:

Received 15 April 2018

Accepted 31 July 2018

Available online 8 August 2018

Keywords:

Mass spectrometry
Histones H3 and H4
 γ H2AX
DNA damage
Embryonic stem cells
Epigenetics

ABSTRACT

Histone posttranslational modifications regulate diverse nuclear functions, including DNA repair. Here, we use mass spectrometry, western blotting, immunohistochemistry and advanced confocal microscopy in order to show radiation-specific changes in the histone signature. We studied wild-type mouse embryonic stem cells (mESCs) and mESCs with a depletion of histone deacetylase 1 (HDAC1), which plays a role in DNA repair. Irradiation by γ -rays increased the S139 phosphorylation of histone H2AX but reduced the level of the H3K9-R17 peptide, which contains S10 phosphorylation (H3S10ph). On an individual cellular level, H3S10ph was low in highly γ H2AX-positive UV laser-induced DNA lesions, and this nuclear distribution pattern was not changed by HDAC1 depletion. Despite this fact, spontaneous γ H2AX-positive DNA lesions colocalized with large H3S10ph-positive nuclear bodies that appear in the G2 phase of the cell cycle. Similarly, by FLIM-FRET analysis, we observed an interaction between H3S10ph and γ H2AX in the G2 phase. However, this interaction was reduced when cells were exposed to γ -rays. A mutual link between H3S10ph and γ H2AX was not observed in the G1 phase of the cell cycle. Together, our data show that despite the fact that H3S10ph is not directly involved in DNA repair, a decrease in H3S10 phosphorylation and weakened interaction between H3S10ph and γ H2AX is a result of radiation-induced damage of the genome. In this case, γ -irradiation also decreased the number of cells in the G1 phase, characterized by no interaction between H3S10ph and γ H2AX.

© 2018 Elsevier B.V. and Société Française de Biochimie et Biologie Moléculaire (SFBBM). All rights reserved.

List of abbreviations: FLIM, Fluorescence lifetime image microscopy; FRET, Förster resonance energy transfer; H3, histone H3; H4, histone H4; me1, monomethylated histones; me2, dimethylated histones; me3, trimethylated histones; H3K9me1/me2/me3, histone H3 methylated on lysine 9 (mono-, di-, trimethylation); H3K9ac, histone H3 acetylated on lysine 9; HDAC1, histone deacetylase 1; HRR, homologous recombination repair; IRIF, γ -irradiation-induced foci; NHEJ, nonhomologous end joining; γ H2AX, S139 phosphorylated histone H2AX; Sph, serine phosphorylation; Kac, lysine acetylation; PTM, posttranslational modification.

* Corresponding author. Institute of Biophysics of the Czech Academy of Sciences, Královopolská 135, CZ-612 65, Brno, Czech Republic.

E-mail address: bartova@ibp.cz (E. Bártová).

¹ designates co-first authors.

1. Introduction

Studies on epigenetic features, including histone post-translational modifications, are essential for understanding the regulation of nuclear processes, such as replication, transcription, splicing and DNA repair. Epigenetic events play a role especially in the regulation of gene expression; however, DNA repair pathways are also mediated by specific histone signatures. For example, the functions of the following markers are very important: S139 phosphorylation of histone H2AX (hereinafter γ H2AX), ubiquitination of H2AX on lysine 15, H3K9 trimethylation, H3K79 monomethylation, or H4K20 dimethylation [1–6].

It is well known that these epigenetic events proceed irrespective of changes in primary DNA sequences [7]. From the perspective of potential therapeutic applications, it is important

that epigenetic markers are reversible to a large extent. For example, clinically used inhibitors or activators of epigenetically important enzymes, including histone deacetylases (HDACs) or DNA methyltransferases (Dnmts), are therapeutically significant, especially in cancer treatment [8,9]. The regulatory roles of histone acetylation and DNA methylation are primarily exerted in gene promoter regions; thus, the physiological functions of histone acetyltransferases (HATs), histone deacetylases (HDACs) and Dnmts are essential [10–12]. A very important regulatory role is also attributed to di/trimethylation of histone H3 at the lysine 9 position (H3K9me2/me3). Methylation of H3K9 is mediated by specific methyltransferases (HMTs) that are responsible for gene silencing and heterochromatin formation [13]. H3K9me3-positive heterochromatin represents a binding site for isoforms of heterochromatin protein 1 (HP1 α , HP1 β , and HP1 γ), which are recruited to UV-induced DNA lesions [14,15]. Moreover, Sun et al. [16] showed an interaction between H3K9me3 and the acetyltransferase Tip60 that regulates DNA repair. A decrease in H3K9me3 suppresses activation of Tip60's acetyltransferase activity, which leads to dysfunction of a key DNA repair-related kinase, ATM (ataxia telangiectasia mutated) [16]. Therefore, erroneous repair of double-strand breaks (DSBs) can appear in cells with an abrogation in the mechanism leading to H3K9 methylation. However, an exact regulatory role of H3K9 methylation in DNA repair is not fully established because some data are controversial. Ayrapetov et al. [17] showed the very interesting phenomenon that Suv39h1, a methyltransferase responsible for H3K9 methylation, is recruited to DSBs in order to stabilize damaged chromatin and activate ATM. This mechanism is essential for chromatin remodeling and for the formation of γ H2AX-positive, irradiation-induced foci (IRIF) [18].

In addition to H3K9 methylation and γ H2AX, histone acetylation is also very dynamic at damaged chromatin. Recently, we showed that UVA-induced DNA lesions lack H3K9 acetylation, which was accompanied by the recruitment of HDAC1 to locally microirradiated chromatin in mouse embryonic stem cells [19]. Guo et al. [20] showed that UV-irradiation affects H3K9 and H4K16 acetylation and that many changes in histone acetylation profiles are induced in parallel with the appearance of cyclobutane pyrimidine dimers (CPDs). Thus, the nucleotide excision repair (NER) pathway is regulated via histone acetylation or deacetylation [21]. From this view, functions of HATs and HDACs appear to be essential for faultless DNA damage response (DDR). Interestingly, in cells exposed to radiation, histone H2AX can be not only phosphorylated on serine but also acetylated on lysine 5, which is mediated via the histone acetyltransferase Tip60. This epigenetic event is a prerequisite for mono- and poly-ubiquitination of H2AX on lysine 119, which is independent of γ H2AX [22]. Another example of a DDR-related epigenetic event is H3K14 hyperacetylation, which appears after irradiation in an experimental system published by Ref. [23]. Similarly, Shogren-Knaak et al. [24] showed that H4K16ac regulates the DNA damage response via chromatin relaxation at DNA lesions. This process was linked to the function of the histone acetyltransferase MOF1, and depletion of this enzyme caused an accumulation of 53BP1, MDC1 or BRCA1 repair proteins to DNA lesions. On the other hand, the γ H2AX level remains unchanged [25–27]. Interestingly, H4K16 acetylation is important for an interaction between the well-known markers of DNA lesions, γ H2AX and MDC1 protein [25]. Thus, in general, a balance between histone acetylation and deacetylation regulates proteins involved in the DNA repair machinery.

Much attention has also been dedicated to histone H3 phosphorylation, which regulates mitotic chromosome condensation [28,29]. In this case, H3 phosphorylation appears on serines 10 and 28 or threonines 3 and 11 [30,31]. From the perspective of DNA repair, phosphorylation of H2AS129 was detected at sites of DNA damage in yeasts [32–34]. It was shown that this posttranslational modification

spreads ~50 kilobases around a given DNA break, while the main mammalian epigenetic marker of DSB sites, H2AX phosphorylated on Serine 139, spreads over megabases [34–36]. <https://www.ncbi.nlm.nih.gov/pmc/articles/PMC3469451/> R16 These histone markers represent homologous sites that serve mostly the same function. Yeast H2A is shorter but the c-terminus is very similar to the c-terminus of mammalian H2AX: “KATKASQEL” vs. “KATQASQEY” (see <http://www.rcsb.org/structure/3T7K> and <http://www.rcsb.org/structure/3SHV>). According to these data, it is evident that yeasts are characterized by specific DNA repair-associated epigenetic mechanisms that involve the function of H2AS129ph and H4 phosphorylation on serine 1 (H4S1ph) but many regulatory aspects of repair processes are identical with mammals. Casein kinase II (CKII), an important enzyme participating in DNA repair pathways, is responsible for mentioned H4S1ph, which is potentiated by genotoxic stress [37,38]. Moreover, during DDR-related processes, H2AS129ph acts together with H2AS122ph [39,40]. Therefore, based on these observations, it appears to be evident that histone phosphorylation, in general, is a fundamental epigenetic regulator of DNA repair processes.

A mutual balance between specific histone markers is essential for optimal DNA repair. Here, we address how HDAC1 depletion in mouse embryonic stem cells (mESCs) can affect the histone signatures at locally UVA-induced DNA lesions and after cells were exposed to γ -rays. We tested this hypothesis because HDAC1 and HDAC2 represent important epigenetic factors regulating the DNA damage response [26]. We mainly compared the epigenetic profiles of histones H3 and H4 in wild-type (wt) and HDAC1 double-knockout (dn) ES cells exposed to γ -rays. We observed that a decrease in H3S10 phosphorylation is a hallmark of γ -irradiated ESCs, however, radiation-induced changes in H3S10 phosphorylation were not affected by HDAC1 depletion. Changes in H3S10ph were likely caused by a γ -radiation-induced decrease in the number of cells in the G1 phase, characterized by no interaction between H3S10ph and γ H2AX. However, an interaction of such modified histones we found in the G2 phase of the cell cycle.

2. Materials and methods

2.1. Cell cultivation

Wild-type mESCs and HDAC1 dn mESCs were a generous gift from Dr. Christian Seiser, Max F. Perutz Laboratories, Vienna Bio-center, Austria. Mouse ESCs were cultivated in Dulbecco's modified Eagle's medium (DMEM; #D6429, Sigma Aldrich, Czech Republic) supplemented with 15% fetal bovine serum (#10439024, Thermo Fisher Scientific, Czech Republic), 0.1 mM nonessential amino acids (NEAA; #11140035, Thermo Fisher Scientific), 100 μ M 1-thioglycerol (MTG; #M6145, Sigma Aldrich) 1 ng/mL leukemia inhibitory factor (LIF; #ESG1107, Merk, Czech Republic), 10,000 IU/mL penicillin, and 10,000 μ g/mL streptomycin. Matrigel (#354277, Corning, USA) was used for coating the cultivation dishes, which is necessary for the optimal maintenance of mESC pluripotency. The cells were irradiated at 60–70% confluency by γ -rays (cobalt-60) 24 h (h) after seeding.

HeLa-Fucci cells expressing RFP-Cdt1 in the G1 phase and GFP-geminin in the S/G2/M phases (described in detail by Ref. [41]) were cultivated in DMEM medium supplemented with 10% fetal bovine serum (#FB-1090/500 BioTech, Czech Republic) and the appropriate antibiotics at 37 °C in a humidified atmosphere containing 5% CO₂.

2.2. Western blot analysis of histone posttranslational modifications

Western blot analysis was performed following [42,43]. Protein

loading was calibrated to achieve identical concentrations of total protein. Protein concentration was measured with a μ Quant spectrophotometer (BioTek, USA). For the western blot analysis of histone signatures, we used the following antibodies: anti-H3K9me1 (#ab9045, Abcam, UK), anti-H3K9me2 (#ab1220, Abcam), anti-H3K9me3 (#ab8898, Abcam), and anti-H3K9 acetylation (#06-942, Merk). We also used an antibody against histone H2AX phosphorylated at the S139 position (γ H2AX, #ab2893, Abcam), HP1 β (#MAB3448, Merk) and anti-Histone H3 (phospho S10) antibody (#ab5176, Abcam). The western blot data were normalized to the amounts of total protein and total histone H3 (#ab1791, Abcam). Primary antibodies were diluted 1:1000–1:2500; as secondary antibodies, we used goat anti-rabbit IgG (#AP307P, Merk; 1:2000), rabbit anti-mouse IgG (#A9044, Sigma-Aldrich; 1:2000), and goat anti-mouse IgG1 (#sc-2060, Santa Cruz Biotechnology, USA; 1:500). The western blot data (density of western blot bands) were quantified by ImageJ software (NIH freeware) and Student's *t*-test was used for statistical analysis (Sigma Plot software, Jandel Scientific, USA). Statistical significance at $p \leq 0.05$ is shown by (*).

2.3. Irradiation by γ -rays, local microirradiation by UVA laser and confocal microscopy

Mouse ES cells were irradiated with 5 Gy of γ -rays. The irradiation source was cobalt-60 (Chisostat, Chirana, Czech Republic). The cells were harvested 2 h after irradiation and fixed for further analysis by western blots, immunofluorescence, and confocal microscopy.

Potential protein recruitment to DNA lesions was analyzed using the time-lapse mode of a Leica TCS SP5 X confocal microscope (Leica Microsystems, Germany). A UVA laser (355 nm wavelength, Coherent, Inc., USA) was used for local microirradiation of the region of interest (ROI). Cells were cultivated on μ -Dish 35 mm Grid-500 dishes (#81166, Ibidi, Germany). At 60–70% confluence, the cells were sensitized for 16–18 h with 10 μ M 5-bromo-2'-deoxyuridine (BrdU, #11296736001, Sigma Aldrich) according to [44]. We induced local DSBs in the cell nuclei with 100% laser output for 4 s. On microscope stage, cells were cultivated in an incubation hood (EMBL, Heidelberg, Germany) at 37 °C, supplement with 5% CO₂. Image acquisition for the induction of DSBs was performed with the following settings: 512 \times 512 pixels, 400 Hz, bidirectional mode, zoom 8–12. Micro-irradiated cells were fixed in 4% formaldehyde and an immunofluorescence staining was performed. After the staining procedure, the cells were observed on microscope slides according to the coordinates of the microscope stage and grids on the microscopy dishes, and images were acquired with a frame resolution of 1024 \times 1024 pixels.

We also performed 3D-confocal sectioning with the following settings: 30–35 confocal sections with an axial step of 0.3 μ m. The LEICA LAS AF software was used for image acquisition and the fluorescence intensity analysis was performed using ImageJ software (NIH freeware). The degree of colocalization between the proteins of interest was studied using the LEICA LAS AF software colocalization tool.

2.4. Immunofluorescence

Cells were fixed in 4% formaldehyde for 10 min at room temperature. Permeabilization of the cell nuclei was performed by incubation with 0.2% Triton X-100 (#194854, MP Biomedicals, USA) for 10 min and 0.1% saponin (#S7900, Sigma Aldrich) for 12 min. Next, the slides were washed twice in phosphate-buffered saline for 15 min; 1% bovine serum albumin (BSA; #A2153-506, Sigma Aldrich) dissolved in PBS was used as a blocking solution. The samples were incubated in blocking buffer for 1 h and then washed

for 15 min in PBS. For immunofluorescence analysis, we used the following antibodies: anti- γ H2AX (#ab26350, Abcam) and anti-Histone H3 (phospho S10) antibody (#ab5176, Abcam). The primary antibodies were diluted 1:100 in PBS containing 1% BSA. As secondary antibodies, we used Alexa Fluor[®]594-conjugated donkey anti-rabbit IgG (H + L) (#A21207, Thermo Fisher Scientific), Alexa Fluor[®]594-conjugated donkey anti-mouse IgG (H + L) (#A21203, Thermo Fisher Scientific), Alexa Fluor[®]488-conjugated goat anti-mouse IgG (H + L) (#A11029, Thermo Fisher Scientific) and Alexa Fluor[®]647-conjugated donkey anti-rabbit IgG (H + L) (#A31573, Thermo Fisher Scientific). The secondary antibodies were diluted 1:200 in PBS containing 1% BSA. The cell nuclei were visualized using 4',6-diamidino-2-phenylindole (DAPI; #D9542, Sigma Aldrich, Czech Republic) dissolved in Vectashield (H-1000, Vector Laboratories, USA).

2.5. Histone preparation for LC-MS/MS analysis

Histones were isolated as described by Ref. [45]. Briefly, cells were washed twice with ice-cold PBS, resuspended in lysis buffer (80 mmol L⁻¹ NaCl, 20 mmol L⁻¹ EDTA, 1% Triton X-100, 45 mmol L⁻¹ sodium butyrate, and 100 mmol L⁻¹ phenylmethanesulfonyl fluoride [PMSF]), incubated for 20 min on ice, and centrifuged at 2000 g for 8 min. The pellets were resuspended in 900 μ L ice-cold 0.2 mol L⁻¹ H₂SO₄ and incubated for 2 h with shaking at 4 °C. After centrifugation at 16,000 g, the proteins were precipitated from the supernatant with trichloroacetic acid at a final concentration of 25% and incubated for 30 min on ice. After centrifugation at 5000g for 30 min at 4 °C, the pellet was washed with 50 mmol L⁻¹ HCl in acetone, and then with 100% acetone, and subsequently dissolved in water. The protein concentration was determined by Bradford assay (Bio-Rad, USA).

Histone samples of each group represented by two biological replicates (histones isolated from two individual cell cultures of the respective treatment) were subjected to a double round of propionic anhydride derivatization in three technical replicates at both the protein and the peptide levels, as previously described with minor modifications [46,47]. Briefly, a 10 μ g portion of histone sample was diluted with acetonitrile (MeCN) and deionized water to a final volume of 10 μ L and final MeCN concentration of 50% (v/v). NH₄OH (2 μ L) was added, then propionylation reagent was prepared by mixing propionic anhydride with MeCN in a 1:3 ratio and a portion equal to 25% of the sample volume was immediately added. The pH was adjusted to 8–9 by NH₄OH, the sample was incubated in thermomixer at 37 °C and 750 rpm for 20 min, and the sample volume was then reduced in a Savant SPD121P concentrator (SpeedVac; Thermo Fisher Scientific) to 5 μ L. The second round of propionylation was carried out with the same protocol. The propionylated histone proteins were reconstituted in 10 μ L of 100 mM ammonium bicarbonate and trypsin was added in a 1:20 enzyme +: protein ratio. After 2 h digestion at 37 °C, the sample was dried in the SpeedVac. The generated peptides were subjected to a double round of propionylation at the N-termini using the protocol described above. Each sample was dried in a SpeedVac overnight and dissolved in 40 μ L of 50% MeCN. The resulting solution was concentrated in the SpeedVac to 10 μ L. Prior to LC-MS/MS analysis, the sample was acidified by adding formic acid (FA) to a final concentration of 1%.

The samples for phosphorylation analysis were prepared as follows. A 150 μ g portion of histone sample was diluted with acidified acetonitrile solution (80% acetonitrile, 2% FA). MS Phospho-mix standards (MSP1L, MSP2L, and MSP3L; Merck, Czech Republic) were added to the samples. Phosphopeptides were enriched using the Pierce Magnetic Titanium Dioxide Phosphopeptide Enrichment kit (#88811, Thermo Fisher Scientific, USA) according to the

manufacturer's protocol. The eluates were concentrated under vacuum to 3 μ L, diluted with 90 μ L of 0.1% FA and purified using a Hypersep SpinTip C-18 column (Thermo Fisher Scientific).

2.6. Analysis of histone acetylation state by LC-MS/MS

Histone peptides were analyzed by LC-MS/MS using an RSLCnano system (Thermo Fisher Scientific, USA) connected online to an Impact II Ultra-High Resolution Qq-Time-Of-Flight mass spectrometer equipped with a CaptiveSpray nanoBooster ion source (Bruker, USA). First, 100 ng portions of peptides were concentrated online on a trapping column (100 μ m \times 30 mm) filled with 3.5- μ m X-Bridge BEH 130 C18 sorbent (Waters, USA) that had been equilibrated (together with the analytical column) with the initial mobile phase before injecting the sample into the sample loop. The peptides were then separated using an Acclaim Pep-map100 C18 column; 3 μ m particles, 75 μ m \times 500 mm analytical column (#164570, Thermo Fisher Scientific). The gradient elution was as follows: 0–90 min, 1–70% B; 90–100 min, 70–98% B; and 100–120 min, 98% B (where the mobile phases A and B consisted of 0.1% FA in water and in 80% MeCN, respectively) with a flow rate of 300 nL/min. After each injection, the flow rate was set at 4 μ L/min for 6 min to load the peptides on the trap column. The analytical column's outlet was directly connected to the NanoBooster ion source, which was filled with MeCN.

MS and MS/MS spectra were acquired in a data-dependent strategy with a 3 s cycle time. The mass range was set to 150–2200 m/z and precursors were selected from 300 to 2000 m/z . The acquisition speeds of the MS and MS/MS scans (the latter varied according to precursor intensity) were 2 and 4–16 Hz, respectively. Data analysis software (version 4.2 SR1; Bruker, USA) was used for preprocessing the mass spectrometric data (including recalibration, compound detection, and charge deconvolution).

An in-house Mascot search engine (version 2.4.1; Matrixscience, USA) was used to search for matches to exported MS/MS spectra obtained from analyses of the samples in in-house histone *Mus musculus* (version 2017-02; 96 protein sequences in total) and cRAP contaminants databases. Settings for all searches included semi-specific Arg-C enzyme specificity and up to two missed cleavages. The following variable modifications were set for searches against the histone *Mus musculus* database: methyl (R, K), dimethyl (K), trimethyl (K), propionyl (K, N-term, S, T, Y), acetyl (K, protein N-term) and phosphorylation (S, T). Propionyl (K, N-term), acetyl (K, protein N-term), oxidation (M) and de-amidation (N, Q) were selected for cRAP database searches. The mass tolerances of the peptides and MS/MS fragments for MS/MS ion searches were 7 ppm and 0.03 Da, respectively. Manual peak labeling and calculation of the peak area corresponding to each precursor ion from the extracted ion chromatograms (XICs) were done via Skyline 3.6 software. A spectral library was created using the Proteome Discoverer platform (version 1.4; Thermo Fisher Scientific). Only peptides with statistically significant peptide scores ($p < 0.01$) were included. Rank 1 peptides with Mascot expectation values < 0.01 and at least six amino acids were considered. The relative abundance (RA) of specific modified histone forms was calculated according to the following formula:

$$RA = \frac{\sum \text{peak areas of XICs of peptides with certain PTM}}{\sum \text{peak areas of XICs of all forms of the peptide}}$$

2.7. Analysis of histone phosphorylation state by LC-MS/MS

Phospho-enriched histone peptides were analyzed by LC-MS/

MS as described earlier by Ref. [48] with minor modifications in the gradient elution: 1% B for 16 min at 600 nL/min to concentrate peptides, then (with a switch to 300 nL/min) 1–13% B over 20 min, 13–33% B over 25 min, 33–56% B over 20 min and 56–80% B over 5 min, followed by isocratic washing at 80% B for 5 min (where the mobile phases A and B consisted of 0.1% FA in water and in 80% MeCN, respectively).

The RAW mass spectrometric data files were analyzed using the Proteome Discoverer software (version 1.4; Thermo Fisher Scientific) with an in-house Mascot search engine to compare the acquired spectra with entries in the in-house histone *Mus musculus* database. The settings for all of the searches included trypsin enzyme specificity and up to five missed cleavages. The following variable modifications were set for searches: methyl (R, K), dimethyl (K), trimethyl (K), acetyl (K, protein N-term) and phosphorylation (S, T, Y). The mass tolerances of peptides and MS/MS fragments for the MS/MS ion searches were 7 ppm and 0.03 Da, respectively. Manual peak labeling and calculation of the peak area corresponding to each precursor ion from the extracted ion chromatograms (XICs) were performed via the Skyline 3.6 software. A spectral library was created using the Proteome Discoverer platform (version 1.4; Thermo Fisher Scientific). Only peptides with statistically significant peptide scores ($p < 0.01$) were included. Rank 1 peptides with Mascot expectation values < 0.01 and at least six amino acids were considered. Peptide identifications were manually verified, and quantitative data were evaluated using the Skyline 3.6 software. The precursor areas of phosphorylated histone peptides were normalized to the signals of the MS Phosphomix standards.

2.8. Cell cycle analysis by flow cytometry

Cells were harvested 2 h after irradiation by 5 Gy of γ -rays. The cells were resuspended in 0.5 ml PBS (4 °C) and fixed by 70% ethanol at 4 °C for at least 30 min. Staining of cell nuclei was performed with Vindelov's solution (10 mM Tris, 0.7 mg/ml RNase, 0.1% Triton X-100, 0.05 mg/ml propidium iodide; PI) at 37 °C for 30 min. Cell cycle parameters (the numbers of cells in the individual cell cycle phases) were measured using a BD FACSVerser flow cytometer (BD Biosciences, USA) equipped with a 488-nm laser. The FACSuite (BD Biosciences) and ModFit software (Verity Software House, USA) were used for measurement and analysis of the percentages of cells in the G1, S and G2-M phases of the cell cycle. All of the analyses were performed on three independent biological replicates.

2.9. Immunoprecipitation (IP)

Immunoprecipitation was performed according to [49]. Analyses were performed in wt and HDAC1 dn mESCs. The cells were grown to 70% confluence, and 24 h after seeding, the cells were irradiated with 5 Gy of γ -rays delivered by cobalt-60 (^{60}Co ; Chisostat, Chirana, Czech Republic; see Ref. [50]). Two hours after γ -irradiation, irradiated and non-irradiated cells were washed in cold PBS buffer and incubated on ice for 5 min in Pierce™ IP Lysis Buffer (# 87788, Thermo Fisher Scientific) supplemented with a protease and phosphatase inhibitor cocktail (#78440, Thermo Fisher Scientific). The total protein concentration was determined using the DC Protein Assay kit (#5000111, Bio-Rad, Bio-Consult, Czech Republic) and an ELISA Reader μ Quant (BioTek, USA). Immunoprecipitation was performed according to the manufacturer's protocol (Catch and Release®v2.0 Reversible Immunoprecipitation System, #17-500, Millipore, USA). Briefly, spin columns with resin were washed twice with 1x wash buffer. Next, the reagents were added to spin columns in the following order: 1x wash buffer, cell lysate, specific

primary antibody [anti-Histone H3 (phospho S10) antibody (#ab5176, Abcam)] or negative control antibody (IgG whole molecule, #A4914, Sigma-Aldrich) and antibody capture affinity ligand. The immunoprecipitation reactions were performed overnight at 4 °C. The next day, the spin columns were washed three times with 1x wash buffer, and the proteins were eluted from the columns with 1x denaturing elution buffer containing β -mercaptoethanol (to a final concentration of 5%). The precipitates were fractionated by SDS-PAGE and analyzed by western blot. For western blotting, we used an anti- γ H2AX antibody (#ab2893, Abcam), and the immunoprecipitation analyses were performed in three biological replicates.

2.10. FLIM-FRET analysis

Fluorescence lifetime image (FLIM) microscopy combined with Förster resonance energy transfer (FRET) was performed following [51]. We used the FRET-FLIM technique to study the interaction between γ H2AX and H3S10ph. We measured a decrease of the fluorescence lifetime of the donor (τ_D) in fixed cells after immunostaining. In our experiments, we used Alexa 488-visualized γ H2AX (donor-only) or Alexa 488-visualized γ H2AX and Alexa 594-visualized H3S10ph (donor-acceptor pair). For the FLIM measurements, we used a Leica TCS SP8 X SMD confocal microscope (Leica Microsystems GmbH, Germany) with a PicoHarp 300 module (PicoQuant GmbH, Germany) and HyD SMD detectors. For every measurement, we applied identical conditions, e.g., identical laser power and detector setting. For the excitation source, we used a pulsed white light laser (WLL) tuned to 488 nm with a repetition rate of 20 MHz. A 63 \times oil immersion objective of 1.4 numerical aperture was used for photon acquisition. We acquired at least 500 photons/pixel at a resolution of 512 \times 512 pixels. We analyzed the results with SymPhoTime 64 software (PicoQuant GmbH, Germany). FRET efficiency was calculated as the mean fluorescence lifetimes weighted by the amplitudes, according to the formula $E = 1 - (\tau_{DA}/\tau_D)$ [52]. Ten cell nuclei were studied by FRET-FLIM for each experimental event.

3. Results and discussion

3.1. H2AX hyperphosphorylation induced by γ -irradiation was accompanied by a decrease in H3S10 phosphorylation

Here, we analyze posttranslational histone modifications in non-irradiated and γ -irradiated wt and HDAC1 double knockout (dn) mouse embryonic stem cells (mESCs). In this experimental model, we show mass spectrometric data of selected peptide forms on the N-termini of histones H3 and H4 (aa sequence regions 9–40 and 4–17, respectively). We found clearly different histone modification patterns in the control (non-irradiated) wt mESCs and HDAC1 dn mESCs. For example, changes in acetylation were represented by increased levels of a doubly acetylated form of H3 K18QLATK23AAR in HDAC1 dn mESCs (Fig. 1A). In detail, there was a 5.3% increase in H3K18acK23ac in HDAC1 dn cells in comparison to wt counterpart (Fig. 1A).

The next analysis showed higher levels of H3 K27SAPATGGVKKPHR40 peptides with K27ac/K36me2 and K27me1 marks, together with a decrease in the abundances of the K36me1 and K36me2 forms, in the control (non-irradiated) HDAC1 dn cells (Fig. 1B). HDAC1 depletion in mESCs also caused changes in the level of the tetra-acetylated form of the H4 G4KGGKGLGKGGAKR17 peptide (K5acK8acK12acK16ac) (Fig. 1C, green rectangle). In this case, there was an increase in the abundance of its form (from 27.8 \pm 0.6% in wt to 32.0 \pm 1.0% in HDAC1 dn cells, respectively). The difference was significant at the level of

$p \leq 0.01$.

The most significant results came from mass spectrometry, where we analyzed H3 phosphorylation in both wt mESCs and HDAC1 dn mESCs. We found that H3K9me3/S10ph, H3K9me2/S10ph/K14ac, H3K9me2/S10ph/K14, H3K9/S10ph/K14ac and H3K9/S10ph/K14 levels were reduced by γ -irradiation (Fig. 2A and B). A decrease in H3S10 phosphorylation was observed to be a key response to γ -irradiation, as evident from more than two-fold decreases in the overall proportion of S10ph-containing peptides in both cell lines. Radiation-induced dephosphorylation of H3S10, analyzed in parallel with the H3K14 acetylation status, was more pronounced in HDAC1-depleted cells compared with that in their wild-type counterpart. We confirmed the given differences in histone signature by Student's t-test (at $p \leq 0.01$). These differences

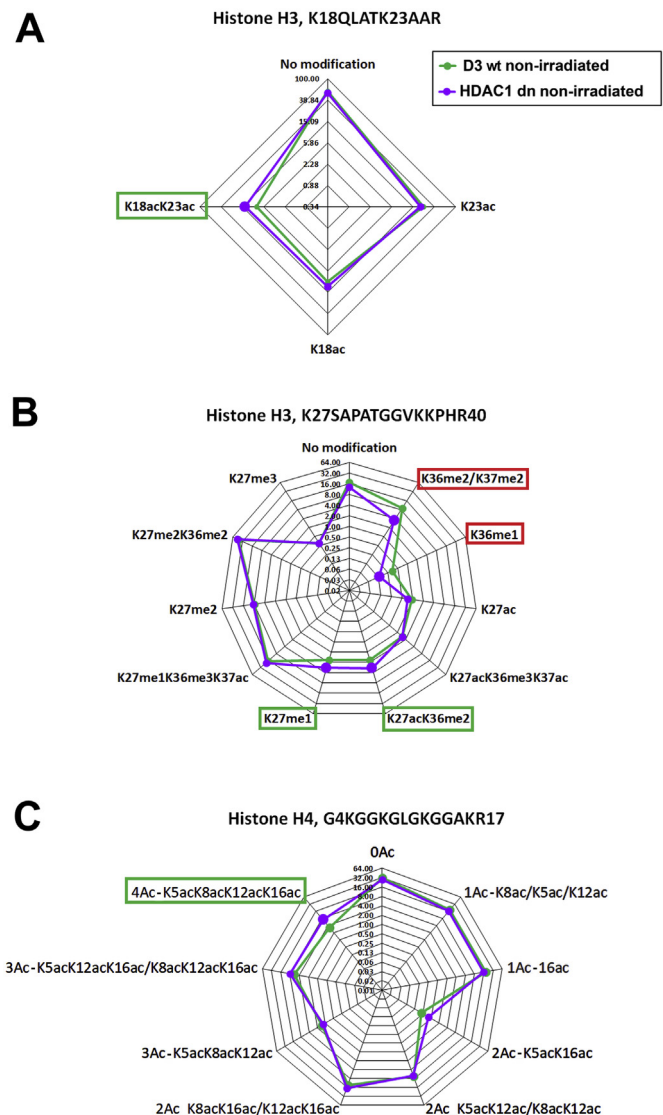


Fig. 1. Differences in the histone modification profiles between non-irradiated wild-type and HDAC1 double knockout mouse ESCs. Radar charts show RAs (means, $N = 6$) of histone H3 and H4 peptide forms (ratios of the XIC peak areas of peptides with given PTMs to the sum of the peak areas of all forms of certain H3 or H4 peptide sequences, respectively, in percentages). The Y axes have a binary logarithmic scale with zero located in the center. Significantly down- and upregulated ($p < 0.01$) isoforms related to HDAC1 depletion are highlighted by red and green rectangles, respectively. The legend in panel (A) is applicable for all panels. Mass spectrometry analyses show results on (A) histone H3, K18QLATK-AAR26 peptide; (B) histone H3, K27SAPATGGVKKPHR40 motif; (C) histone H4, G4KGGKGLGKGGAKR17 motif.

fulfilled the condition of results $>1.5\times / <0.75\times$ when we compared the non-irradiated control cell population with the γ -irradiated samples (Fig. 2A and B). These observations prompted us to further investigate the histone phosphorylation status by extending our MS-based study to include an analysis of phospho-enriched peptides. In both wt and HDAC1 dn cells, we observed a significant γ -radiation-induced increase in serine 139 phosphorylation of histone H2AX (H2A.X KASQAS139phQEY peptide; Fig. 3A). We detected the same trend in the protein levels (although it was not statistically significant) in the case of H2AXS120ph (H2A.X KS120phSATVGPVK). Interestingly, non-irradiated HDAC1 dn cells were characterized by a pronouncedly high level of H2AXS120ph

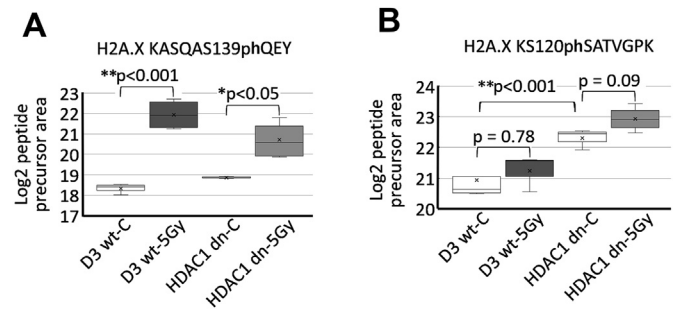


Fig. 3. The proportion of signature marks on the H3K9-R17 peptide in non-irradiated and γ -irradiated wt and HDAC1 dn mESCs. Box-plots of the RAs ratio of specific H3 PTMs showing extremes, interquartile ranges, means and medians (N = 6). Panel (A) shows the H2A.X KASQAS139phQEY motif and panel (B) shows the H2A.X KS120phSATVGPVK motif. Statistically significant results are shown by asterisks in both panels A, B.

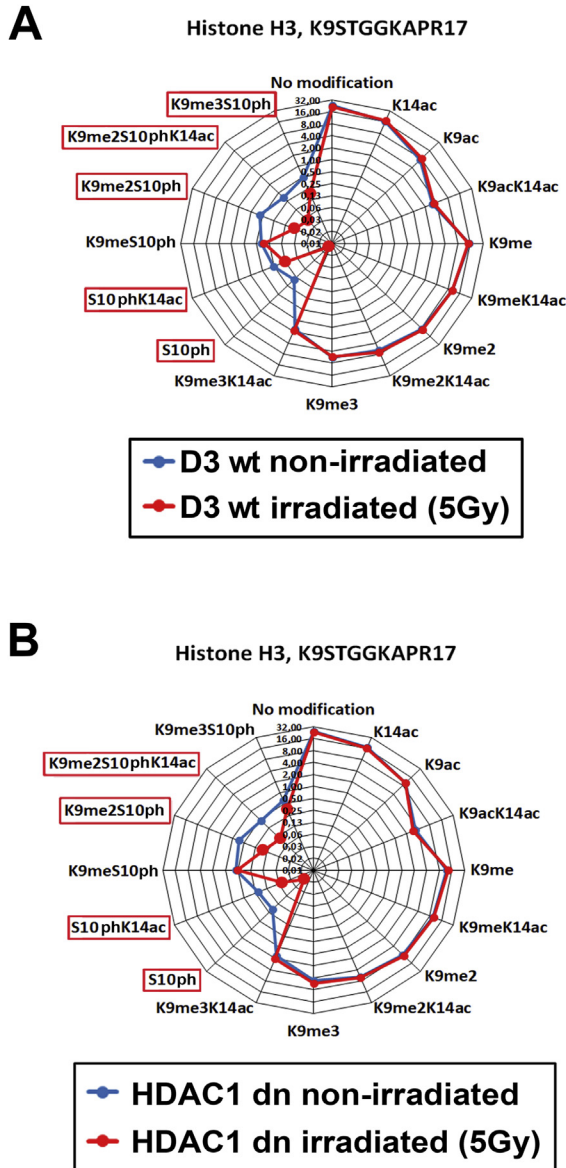


Fig. 2. Posttranslational modifications of histone H3 in non-irradiated and γ -irradiated wild-type or non-irradiated and γ -irradiated HDAC1 double knockout (dn) mouse ESCs (mESCs). Radar charts showing RAs (means, N = 6) of histone H3 peptide forms (ratios of the XIC peak areas of peptides with given PTMs to the sum of the peak areas of all forms of the certain H3 peptide sequence, in percentages). The Y axes have a binary logarithmic scale, with zero located in the center. Significantly downregulated ($p < 0.01$) isoforms by irradiation are highlighted by red rectangles. The panels show posttranslational modifications of the histone H3 K9STGGKAPR17 motif in (A) non-irradiated and γ -irradiated wild-type mESCs, and (B) in non-irradiated and γ -irradiated HDAC1 dn mESCs.

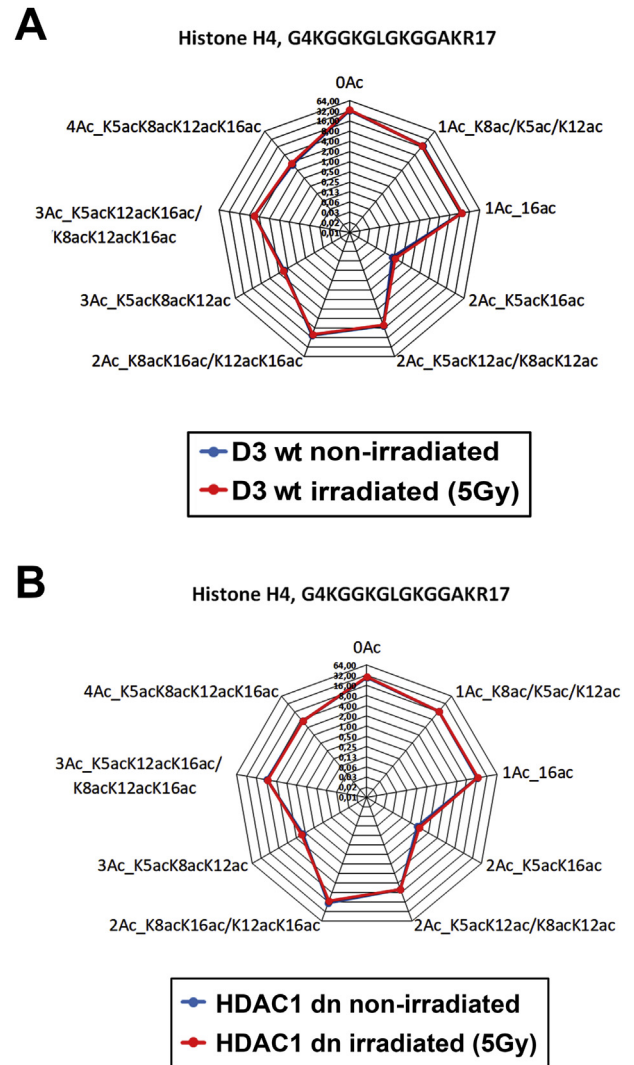


Fig. 4. Mass spectrometry analysis of posttranslational modifications on histone H4 (G4KGGKGLGKGGAKR17 motif) in (A) non-irradiated and γ -irradiated wild-type and (B) in non-irradiated and γ -irradiated HDAC1 dn ESCs. Radar charts showing RAs (means, N = 6) of histone H4 N-terminal peptide forms (ratios of the XIC peak areas of peptides with given PTMs to the sum of the peak areas of all forms of the N-terminal peptide sequence, in percentages). The Y axes have a binary logarithmic scale, with zero located in the center.

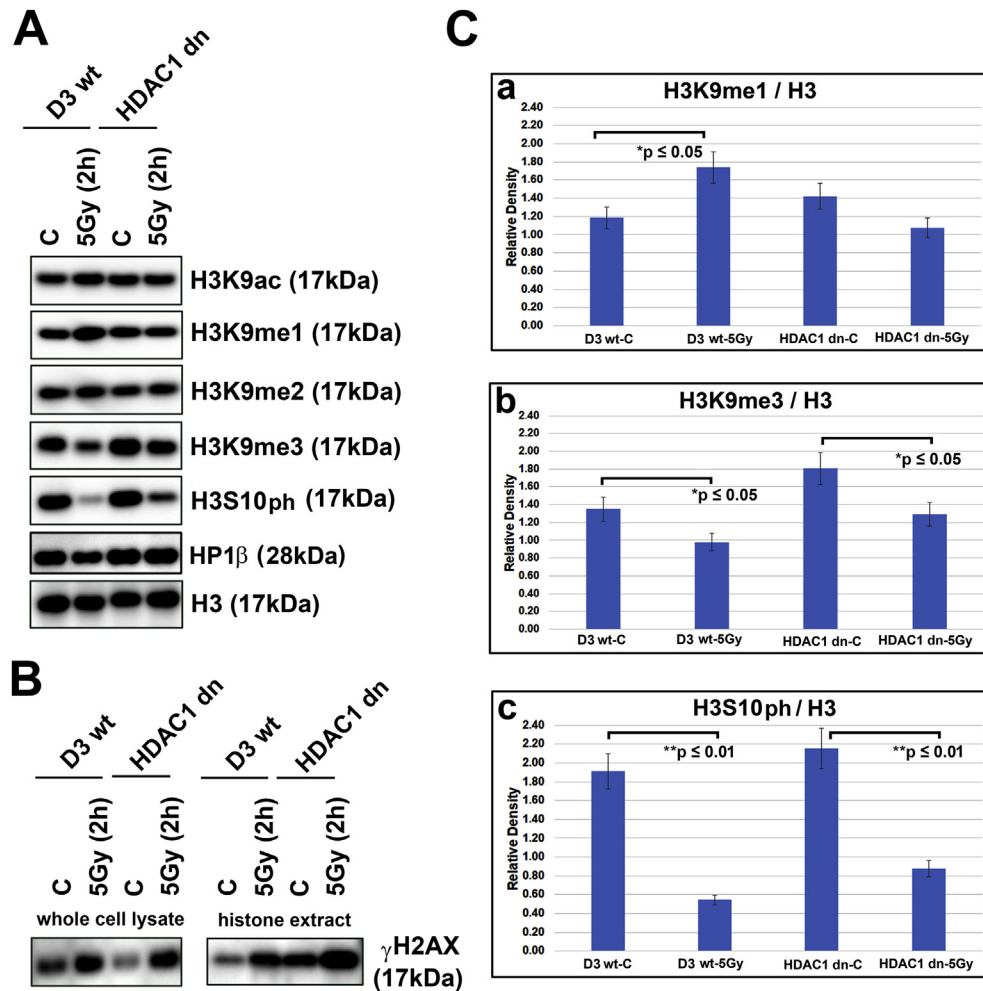


Fig. 5. Western blot analysis of H3K9ac, H3K9me1/me2/me3, H3S10ph, HP1 β , and γ H2AX in non-irradiated and γ -irradiated wt and in non-irradiated and γ -irradiated HDAC1 dn mESCs (**A**, **B**). Significant changes in histone marks are shown in panel (**C**). The western blot data were quantified by ImageJ software and statistically significant results are shown at * $p \leq 0.05$ and ** $p \leq 0.01$. Statistical analysis was performed by applying Student's t-test for (a) H3K9me1, (b) H3K9me3 and (c) H3S10ph.

compared with that of their non-irradiated wt counterparts ($p \leq 0.01$); (Fig. 3B). However, the other epigenetic markers that we studied were not changed when we compared non-irradiated and γ -irradiated wt cells or non-irradiated and γ -irradiated HDAC1 dn mESCs. In this regard, we analyzed epigenetic marks on histones H4 and H3 (Fig. 4A and B, and Supplementary Fig. 1A–D). In the case of histone H3, we studied the following histone posttranslational modifications: K9me3/K14ac, K9me3, K9me2/K14ac, K9me, K9ac/K14ac, K9ac, K14ac, K18ac/K23ac, K18ac, K23ac, K27me3, K27me2/K36me2, K27me2, K27me1/K36me3/K37ac, K27me1, K27ac/K36me2, K27ac/K36me3/K37ac, K27ac, K36me1, K36me2/K37me2 and histones without posttranslational modifications (Supplementary Fig. 1A–D).

In summary, even though H3K14 hyperacetylation was found to be induced by UV damage in yeast and is essential for the repair of UV photolesions [23,53], in our experimental system, the abundances of H3K14ac-peptides without S10ph were not different in wt mESCs and HDAC1 dn cells exposed to γ -rays (Fig. 2A and B). Thus, changes in histone acetylation induced by DNA damage are cell-type- and species-specific. Interestingly, in the literature, the presence of bivalent phosphoacetylation domains was found to be required for transcriptional activation of the *hdac1* gene [54]. Thus, here we would like to suggest that bivalent histone domains (phospho-acetyl, phospho-dimethyl, and phospho-trimethyl)

could play an important role in the DNA damage response (Fig. 2A and B).

3.2. H3S10 dephosphorylation was accompanied by a depletion of H3K9me3 and an increase in H3K9me1 levels in γ -irradiated wild-type mESCs

By western blots, we verified the levels of the histone marks, revealed by mass spectrometry. We focused on H3K9 acetylation, H3K9me1/me2/me3, H3S10ph, HP1 β (as an H3K9me2/me3 binding partner) and γ H2AX in non-irradiated and γ -irradiated wt and HDAC1 dn cells (Fig. 5A–C). We showed that specifically the H3K9me1 level in wt mESCs, but not in HDAC1 dn mESCs, was increased in γ -irradiated cells compared with that of their non-irradiated counterparts (Fig. 5A, Ca). However, H3K9me3 and H3S10ph levels were decreased by γ -irradiation in both wt and HDAC1-depleted cells (Fig. 5A, Cb, Cc). H3S10 phosphorylation was affected to a lesser extent in γ -irradiated HDAC1 dn cells, which corresponds to the MS-based results described above. Interestingly, the level of HP1 β was not changed by irradiation, in comparison with a decrease in H3K9me3 (Fig. 5A). These changes in the histone signature and the related protein HP1 β were accompanied by a radiation-induced level increase in γ H2AX in both wt and HDAC1 dn cells (Fig. 5A and B).

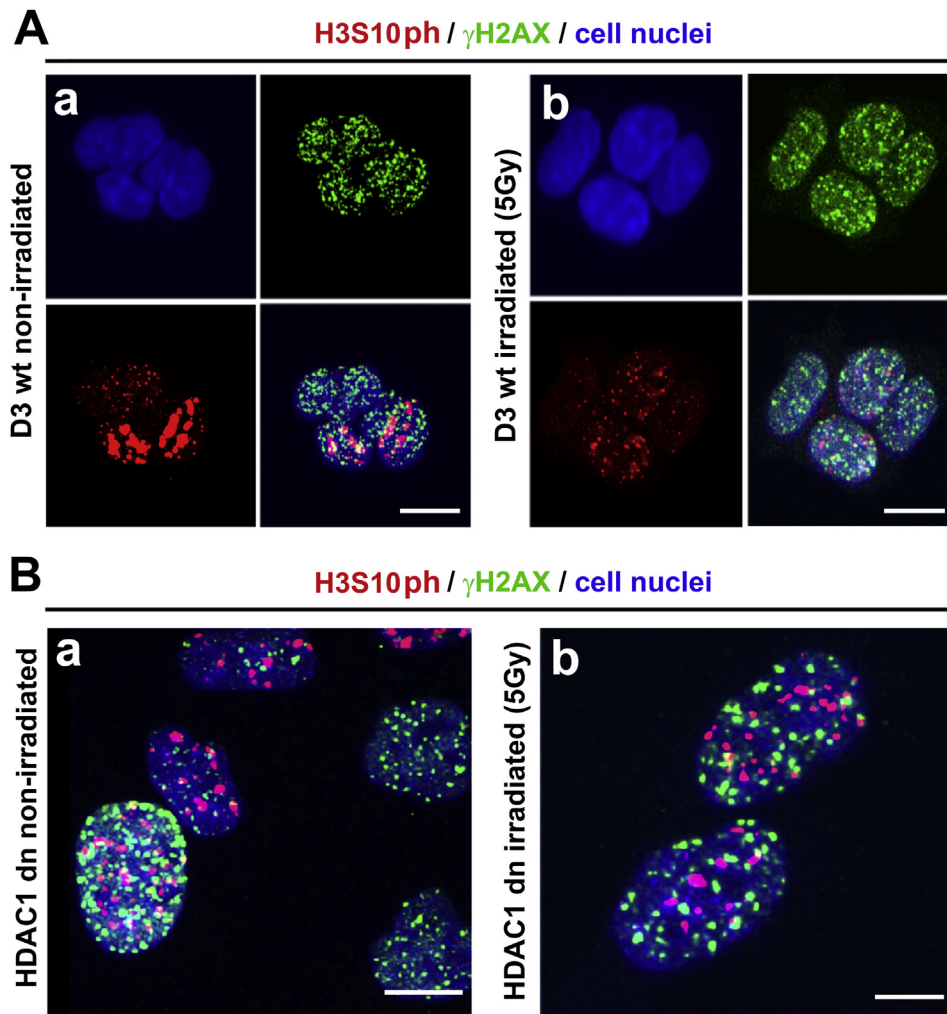


Fig. 6. The nuclear distribution pattern of γ H2AX (green) and H3S10ph (red) in non-irradiated and γ -irradiated (**Aa, Ab**) wt mESCs, and (**Ba, Bb**) in non-irradiated and γ -irradiated HDAC1 dn mESCs. The analysis was performed by immunofluorescence combined with confocal microscopy. The cell nuclei were stained with DAPI (blue fluorescence). The scale bars in panels A, B show 10 μ m.

Changes in H3K9me3 induced by γ -irradiation fit well with the observation of Luijsterburg et al. [15] showing that all HP1 isoforms are recruited to UV-induced DNA lesions independently of H3K9me3. In case of identical functions of H3K9me3 and HP1 isoforms in the DNA damage response, one would rather expect an increase in the H3K9me3 level after cell exposure to genotoxic stress because HP1 accumulates at DNA lesions. In this regard, Ayrapetov et al. [17] published that a protein complex containing H3K9-HMT Suv39h1, Kap-1, and HP1 are rapidly recruited to DNA double-strand breaks. From these results, it seems that the function of H3K9me3-HP1 in DNA repair likely depends on the type of DNA injury. Here we show a DNA damage response in γ -radiated wild-type mESCs, characterized by a depletion in H3K9me3, dephosphorylation of H3S10 which is accompanied by an increase in γ H2AX and H3K9me1 levels. Expected, S/G2-phase dependent increase in histone markers, caused by genome duplication, we mainly observed by western blots in γ H2AX, but for example, H3K9ac and H3K9me2 levels were not affected by cell cycle changes induced by γ -radiation (Fig. 5A and B and cell cycle data mentioned below). These results document that most histone PTMs are insensitive to the cell cycle changes and if a histone PTM changes through the cell cycle it would be likely altered by cell cycle perturbations.

3.3. H3S10ph-positive foci specific for G2-phase colocalized with γ H2AX and an interaction between H3S10ph and γ H2AX was observed in only the G2 phase but not in the G1 phase of the cell cycle

We also used immunofluorescence to study a mutual interaction between H3S10ph-positive and γ H2AX-positive nuclear foci (Fig. 6Aa, Ab, and Ba, Bb). We observed a close association between γ H2AX and H3S10ph foci in cells that appeared to be in the G2 phase of the cell cycle, as indicated by a high level of H3S10ph and by a robust accumulation of this histone marker into clearly visible foci (Fig. 7A and B). Mitotic cells were also characterized by a very high level of H3S10ph. Conversely, in mESCs passing G1 phase, the level of H3S10ph was lower and H3S10ph did not accumulate into well-visible foci (Fig. 7A–C). A mutual link between γ H2AX- and H3S10ph-positive foci in the G2 phase of the cell cycle we also confirmed by 3D-confocal microscopy showing H3S10ph/ γ H2AX colocalization that was also confirmed by software colocalization tool (Fig. 8Aa, b, Ba, b). We observed a $14.7 \pm 6.8\%$ colocalization rate in non-irradiated cells and a $29.8 \pm 10.5\%$ colocalization rate in γ -irradiated mESCs (Fig. 8Ba, b). Because we were aware that foci colocalization did not directly indicate protein-protein interaction, we

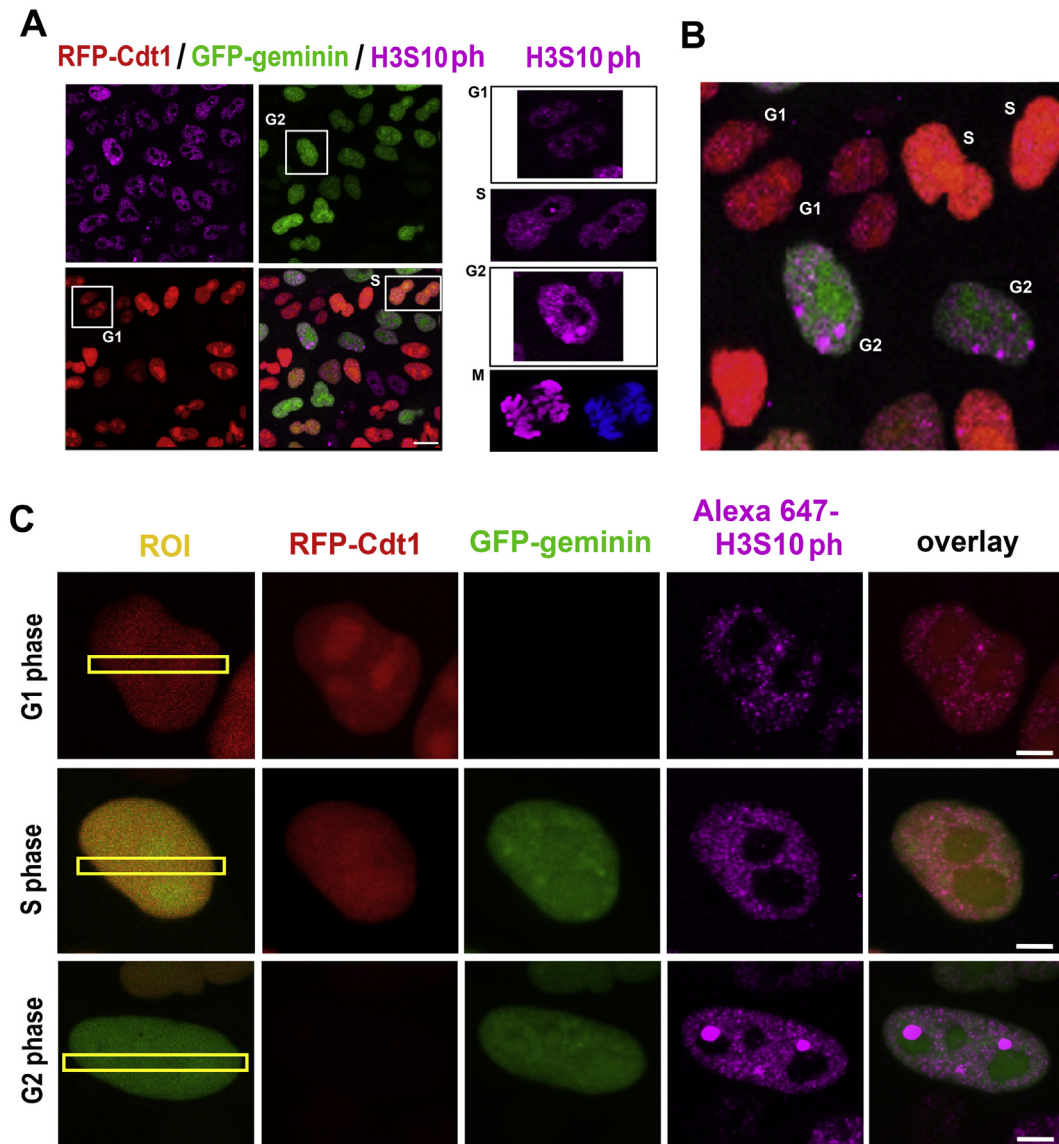


Fig. 7. Levels of H3S10 phosphorylation (violet) studied in the HeLa-Fucci cellular system showing the G1 (RFP-ctd1; red), S (orange; a combination of RFP-Ctd1 and GFP-geminin) and G2 (GFP-geminin; green) phases of the cell cycle. (A–B) The lowest level of H3S10 phosphorylation (violet) was in G1 phase and the highest level was in M-phase of the cell cycle. Focal accumulation of H3S10ph was in G2 phase. The scale bar shows 20 μm. (C) Changes in H3S10ph (violet) were not observed in the UVA-microirradiated chromatin of HeLa-Fucci cells. The G1, S, and G2 phases of the cell cycle were examined. Local microirradiation was performed with a UVA laser (355 nm wavelength). The irradiated regions of interest (ROIs) are shown in yellow rectangles. The scale bars show 5 μm.

also performed immunoprecipitation experiments. This analysis showed a pronounced interaction between the examined histone posttranslational modifications (Fig. 8C). Interestingly, this interaction was weakened when wild-type mESCs and HDAC1 dn cells were exposed to γ -rays (Fig. 8C). Additional FLIM-FRET analysis showed no interaction between H3S10ph and γ H2AX in G1-cells, while cells in the G2 phase of the cell cycle were characterized by a relatively high value of FRET efficiency; $18.2 \pm 4.9\%$ (Fig. 8D). This FRET efficiency confirms the interaction between H3S10ph and γ H2AX in G2 phase of the cell cycle. Our data implied a functional link, affected by γ -irradiation, between the seemingly unrelated histone markers H3S10ph and γ H2AX, which act together in the G2 phase of the cell cycle. However, it is generally accepted that from the view of epigenetic mechanisms, H3S10ph and γ H2AX do not have any direct relationship other than using ATP. From the functional point of view, the bulk

abundance of H3S10ph was decreasing at the same time that it enriched at γ H2AX-positive foci (Fig. 8A). Although the simultaneous decrease in bulk abundance and increase in localization of this mark may seem counterintuitive, histone PTMs often serve different purposes in distinct contexts.

Based on this observation, we also tested if the level of H3S10ph is changed in locally microirradiated genomic regions of wt and HDAC1 dn cells or in HeLa cells (Figs. 7C and 9A, B). We observed that in the G1, S and G2 phases of the cell cycle, the level of H3S10ph was not changed by local microirradiation (Fig. 7C) and that no changes in H3S10ph were found in microirradiated, highly γ H2AX-positive genomic regions in wt and HDAC1 dn mESCs (Fig. 9A and B). Based on these results, we can conclude that H3S10ph is not directly involved in the DNA damage response but that the H3S10ph level and its ability to interact with γ H2AX are changed by γ -irradiation.

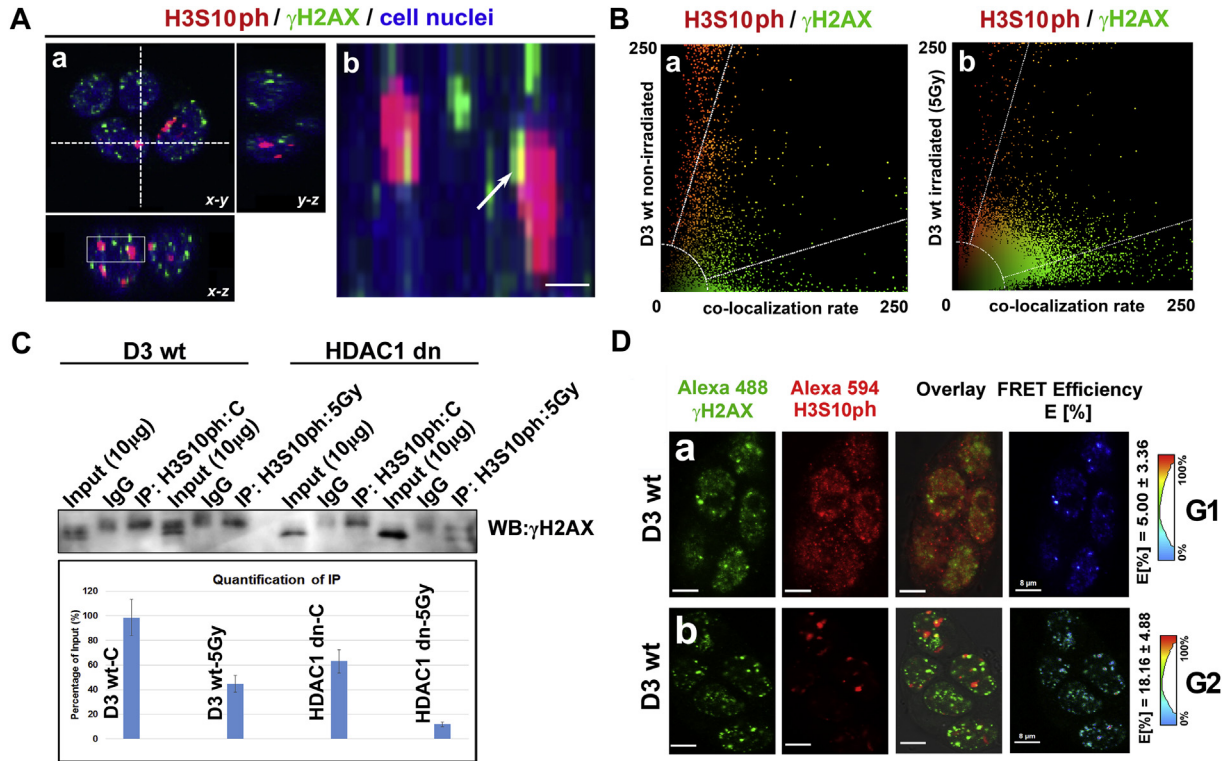


Fig. 8. Colocalization rates between γ H2AX (green) and H3S10ph (red) in non-irradiated and γ -irradiated wt and dn mESCs. Panels (Aa, Ab) show 3D-projections of γ H2AX (green) and H3S10ph (red) in interphase nuclei of wt mESCs. The white arrow shows a colocalization between γ H2AX-positive foci and H3S10ph. The scale bar represents 1 μ m. (B) Colocalization rates (calculated by the Leica software colocalization tool) between γ H2AX and H3S10ph in (a) non-irradiated and (b) γ -irradiated wt mESCs. (C) Immunoprecipitation showed an interaction between γ H2AX and H3S10ph in wt and dn mESCs. This protein-protein interaction was weakened by γ -irradiation. (D) FLIM-FRET analysis showed an absence of an interaction between γ H2AX and H3S10ph in (a) the G1 phase of the cell cycle, but panel (b) shows a degree of an interaction between γ H2AX and H3S10ph in the G2 phase.

3.4. A radiation-induced decrease in the H3S10ph level and a weakened interaction between H3S10ph and γ H2AX caused a radiation-induced cell depletion in the G1 phase

From the perspective of H3S10ph function after DNA damage, we further studied an effect of the cell cycle phases on the nuclear distribution pattern and levels of H3S10ph. By flow cytometry, we showed that γ -irradiation caused an accumulation of cell in the S phase, which appeared at the expense of the G1 phase of the cell cycle. Shortly, in the G1 phase, the number of cells was reduced by γ -radiation (Fig. 10A–E). As mentioned above, the G1 phase is characterized by a lower level of H3S10ph in comparison with that of the G2 phase (Fig. 7A, C). Thus, based on these results, we came to the conclusion that a γ -radiation-induced decrease in H3S10 phosphorylation is not a direct marker of the DNA damage but this effect is caused by γ -radiation-induced changes in the cell cycle profile.

3.5. Conclusions on a function of histone phosphorylation in the DNA damage response

In general, it is well known that histone phosphorylation plays an important role in the DNA damage response. A highly respected epigenetic marker of DSB repair is serine 139 phosphorylation of histone H2AX. Moreover, Allison and Milner [55] specified a role of H3S10 phosphorylation in DNA repair processes. These authors showed that the H3S10ph level is decreased in cells treated with an HDAC inhibitor and exposed to UV light. These data fit well with our observation that H3S10 dephosphorylation is induced after cell exposure to γ -rays. We fully confirm this claim, and, moreover, we clarify a new functionality of H3S10ph. We show an interaction

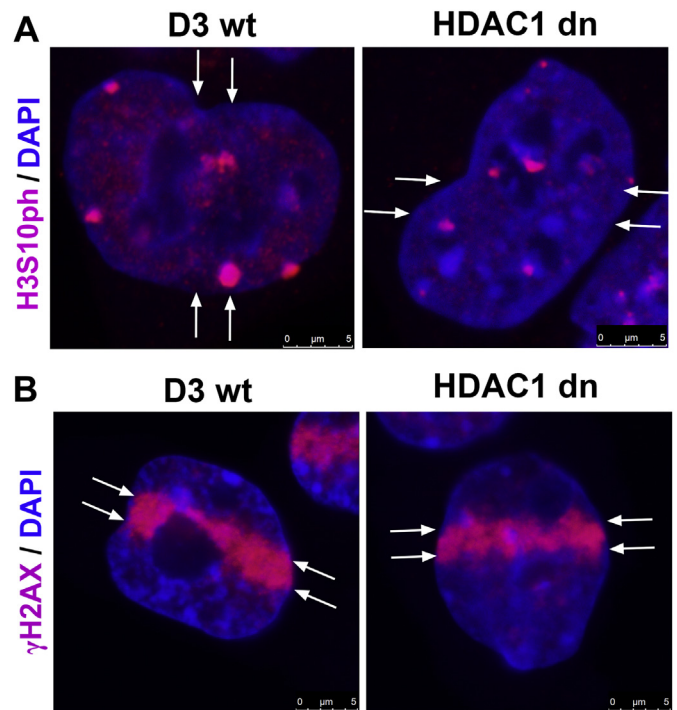


Fig. 9. Levels of γ H2AX and H3S10 phosphorylation on UVA-microirradiated chromatin in wt and HDAC1 dn mESCs. Local microirradiation was performed with a UVA laser (355 nm wavelength). (A) Irradiated ROIs (shown by white arrows) were characterized by a low level of H3S10ph in wt and HDAC1 dn mESC. (B) Hyperphosphorylation of H2AX appeared at microirradiated ROIs delineated by white arrows in both wt and HDAC1 dn mESCs. The scale bars show 5 μ m.

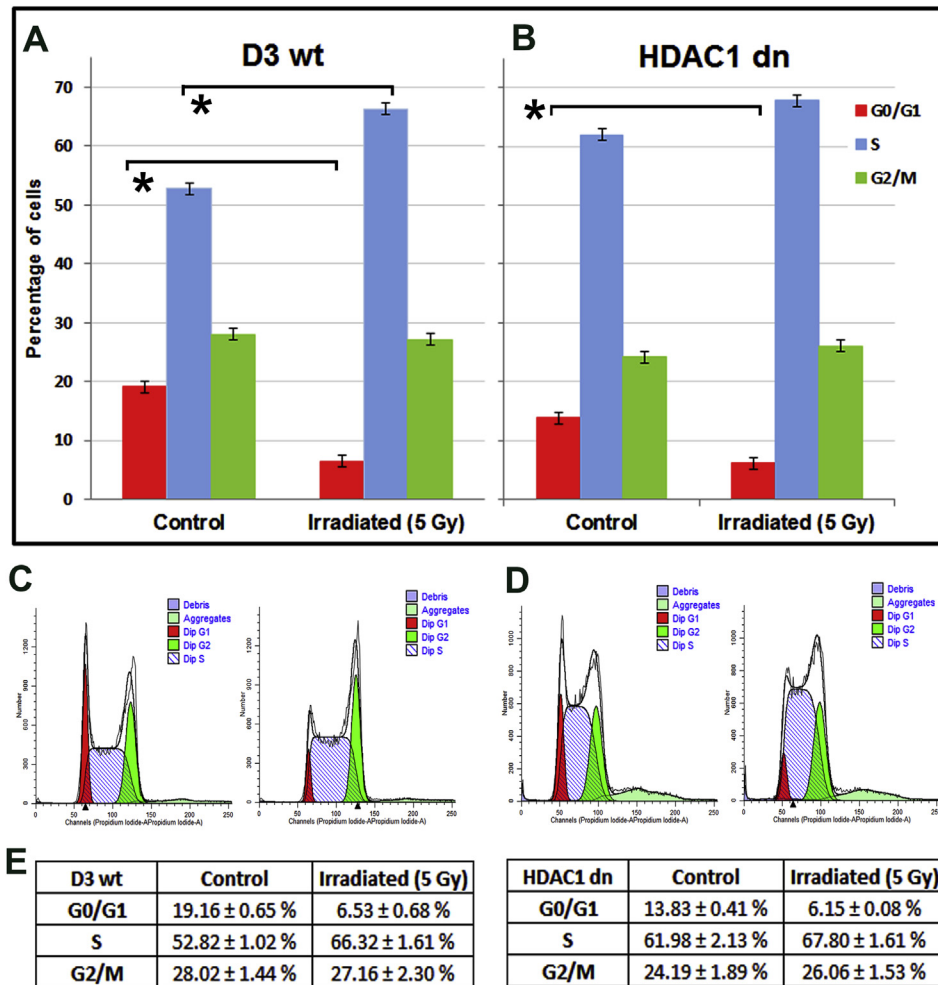


Fig. 10. Cell cycle-dependent profiles measured by flow cytometry in non-irradiated and γ -irradiated wt and HDAC1 dn mESCs. The histograms (bar charts) show the percentages of cells in the G1 (red), S (blue) and G2 (green) phases of the cell cycle in (A) wt ESCs and in (B) HDAC1 dn ESCs. The panels (C, D) show histograms produced by analysis with the ModFit software showing examples of the percentages of cells in the G1 (red peaks), S (dashed blue regions) and G2 (green peak) cell cycle phases. The analyses were performed in (C) non-irradiated and γ -irradiated wt ESCs and in (D) non-irradiated and γ -irradiated HDAC1 dn ESCs. (E) The average numbers of the cells in the individual cell cycle phases are shown in the table.

between H3S10ph and γ H2AX in the G2 phase of the cell cycle. However, this protein-protein mutual interaction was weakened after cell exposure to γ -rays that also reduced the number of cells in the G1 phase. In addition to this observation, we found that G1 cells are characterized by an absence of the interaction between H3S10ph and γ H2AX.

Together, our data show that despite the fact that H3S10ph is not directly involved in DNA repair, radiation-induced changes in the cell cycle can affect the function of H3S10ph. This histone posttranslational modification acts together with γ H2AX in the G2 phase of the cell cycle; thus, H3S10ph presumably contributes to the function of γ H2AX in homologous recombination repair. Banerjee et al. [56] showed that the only one common functional link between histone H2A and H3 exists, and it is ATP hydrolysis that facilitates phosphorylation of these histones and is necessary for chromatin assembly. Thus, here, we document a novel link between H3S10ph and γ H2AX, especially in DNA damage response.

Authors' contribution

EB coordinated the experimental efforts, designed the experiments, finalized all of the images and wrote the paper. SL and JS

were responsible for western blotting, immunofluorescence, confocal microscopy and cell irradiation by Co-60. SL performed IP and FLIM-FRET experiments. RF and JK performed the flow cytometry analysis. GL and ZZ were responsible for the mass spectrometry analysis and the related statistical analysis. All of the authors read and approved the final version of this manuscript.

Funding

This work was supported by the Czech Science Foundation (grant number: 18-07384S). The work was also supported by Strategie AV21, program Qualitas, from the Center of Epigenetics (ICO: 68081707). The CIISB research infrastructure project LM2015043 funded by MEYS CR is gratefully acknowledged for the financial support of the LC-MS/MS measurements at the Proteomics Core Facility. The work was co-funded by the MEYS project CEITEC 2020 (LQ1601).

Conflicts of interest

The authors have declared that there are no conflicts of interest.

Appendix A. Supplementary data

Supplementary data related to this article can be found at <https://doi.org/10.1016/j.biochi.2018.07.029>.

References

- [1] M.V. Botuyan, J. Lee, I.M. Ward, J.E. Kim, J.R. Thompson, J. Chen, G. Mer, Structural basis for the methylation state-specific recognition of histone H4-K20 by 53BP1 and Crb2 in DNA repair, *Cell* 127 (2006) 1361–1373.
- [2] Z. Farooq, S. Banday, T.K. Pandita, M. Altaf, The many faces of histone H3K79 methylation, *Mutat. Res. Rev. Mutat. Res.* 768 (2016) 46–52.
- [3] O. Fernandez-Capetillo, A. Lee, M. Nussenzweig, A. Nussenzweig, H2AX: the histone guardian of the genome, *DNA Repair* 3 (2004) 959–967.
- [4] F. Mattioli, J.H. Vissers, W.J. van Dijk, P. Ikpa, E. Citterio, W. Vermeulen, J.A. Marteijn, T.K. Sixma, RNF168 ubiquitinates K13–15 on H2A/H2AX to drive DNA damage signaling, *Cell* 150 (2012) 1182–1195.
- [5] T. Stiff, M. O'Driscoll, N. Rief, K. Iwabuchi, M. Lobrich, P.A. Jeggo, ATM and DNA-PK function redundantly to phosphorylate H2AX after exposure to ionizing radiation, *Canc. Res.* 64 (2004) 2390–2396.
- [6] M. Zimmermann, T. de Lange, 53BP1: pro choice in DNA repair, *Trends Cell Biol.* 24 (2014) 108–117.
- [7] C. Lahtz, G.P. Pfeifer, Epigenetic changes of DNA repair genes in cancer, *J. Mol. Cell Biol.* 3 (2011) 51–58.
- [8] P.W. Laird, Cancer epigenetics, *Hum. Mol. Genet.* 14 (Spec No 1) (2005) R65–R76.
- [9] J. Peedicayil, Epigenetic approaches for bipolar disorder drug discovery, *Expert Opin. Drug Discov.* 9 (2014) 917–930.
- [10] E. Belikov, L.J. Wong, B.M. Alberts, Extensive purification of histone acetylase A, the major histone N-acetyl transferase activity detected in mammalian cell nuclei, *J. Biol. Chem.* 255 (1980) 11448–11453.
- [11] J.E. Brownell, C.D. Allis, Special HATs for special occasions: linking histone acetylation to chromatin assembly and gene activation, *Curr. Opin. Genet. Dev.* 6 (1996) 176–184.
- [12] N. Martinet, P. Bertrand, Interpreting clinical assays for histone deacetylase inhibitors, *Canc. Manag. Res.* 3 (2011) 117–141.
- [13] C. Baldeyron, G. Soria, D. Roche, A.J. Cook, G. Almouzni, HP1 α recruitment to DNA damage by p150CAF-1 promotes homologous recombination repair, *J. Cell Biol.* 193 (2011) 81–95.
- [14] N. Ayoub, A.D. Jayasekharan, J.A. Bernal, A.R. Venkitesan, HP1 β mobilization promotes chromatin changes that initiate the DNA damage response, *Nature* 453 (2008) 682–686.
- [15] M.S. Luijsterburg, C. Dinant, H. Lans, J. Stap, E. Wiernasz, S. Lagerwerf, D.O. Warmerdam, M. Lindh, M.C. Brink, J.W. Dobrucki, J.A. Aten, M.I. Foustier, G. Jansen, N.P. Dantuma, W. Vermeulen, L.H. Mullenders, A.B. Houtsmuller, P.J. Verschure, R. van Driel, Heterochromatin protein 1 is recruited to various types of DNA damage, *J. Cell Biol.* 185 (2009) 577–586.
- [16] Y. Sun, X. Jiang, Y. Xu, M.K. Ayrappetov, L.A. Moreau, J.R. Whetstone, B.D. Price, Histone H3 methylation links DNA damage detection to activation of the tumour suppressor Tip60, *Nat. Cell Biol.* 11 (2009) 1376–1382.
- [17] M.K. Ayrappetov, O. Gursoy-Yuzugullu, C. Xu, Y. Xu, B.D. Price, DNA double-strand breaks promote methylation of histone H3 on lysine 9 and transient formation of repressive chromatin, *Proc. Natl. Acad. Sci. U. S. A.* 111 (2014) 9169–9174.
- [18] S. Nakamura, I.B. Tanaka 3rd, S. Tanaka, K. Nakaya, N. Sakata, Y. Oghiso, Adiposity in female B6C3F1 mice continuously irradiated with low-dose-rate gamma rays, *Radiat. Res.* 173 (2010) 333–341.
- [19] E. Bartova, G. Sustackova, L. Stixova, S. Kozubek, S. Legartova, V. Foltankova, Recruitment of Oct4 protein to UV-damaged chromatin in embryonic stem cells, *PLoS One* 6 (2011), e27281.
- [20] T. Guo, R. Guan, J.H. Zou, J. Liu, L. Ying, W. Yang, H.B. Wu, Y. Cao, Red light-emitting hyperbranched fluorene-alt-carbazole copolymers with an iridium complex as the core, *Polym Chem-Uk* 2 (2011) 2193–2203.
- [21] M. Brand, J.G. Moggs, M. Oulad-Abdelghani, F. Lejeune, F.J. Dilworth, J. Stevenin, G. Almouzni, L. Tora, UV-damaged DNA-binding protein in the TFIIIC complex links DNA damage recognition to nucleosome acetylation, *EMBO J.* 20 (2001) 3187–3196.
- [22] T. Ikura, S. Tashiro, A. Kakino, H. Shima, N. Jacob, R. Amunugama, K. Yoder, S. Izumi, I. Kuraoka, K. Tanaka, H. Kimura, M. Ikura, S. Nishikubo, T. Ito, A. Muto, K. Miyagawa, S. Takeda, R. Fishel, K. Igarashi, K. Kamiya, DNA damage-dependent acetylation and ubiquitination of H2AX enhances chromatin dynamics, *Mol. Cell Biol.* 27 (2007) 7028–7040.
- [23] M.R. Duan, M.J. Smerdon, Histone H3 lysine 14 (H3K14) acetylation facilitates DNA repair in a positioned nucleosome by stabilizing the binding of the chromatin Remodeler RSC (Remodels Structure of Chromatin), *J. Biol. Chem.* 289 (2014) 8353–8363.
- [24] M. Shogren-Knaak, H. Ishii, J.M. Sun, M.J. Pazin, J.R. Davie, C.L. Peterson, Histone H4-K16 acetylation controls chromatin structure and protein interactions, *Science* 311 (2006) 844–847.
- [25] X. Li, C.A. Corsa, P.W. Pan, L. Wu, D. Ferguson, X. Yu, J. Min, Y. Dou, MOF and H4 K16 acetylation play important roles in DNA damage repair by modulating recruitment of DNA damage repair protein Mdc1, *Mol. Cell Biol.* 30 (2010) 5335–5347.
- [26] K.M. Miller, J.V. Tjeertes, J. Coates, G. Legube, S.E. Polo, S. Britton, S.P. Jackson, Human HDAC1 and HDAC2 function in the DNA-damage response to promote DNA nonhomologous end-joining, *Nat. Struct. Mol. Biol.* 17 (2010) 1144–1151.
- [27] G.G. Sharma, S. So, A. Gupta, R. Kumar, C. Cayrou, N. Avvakumov, U. Bhadra, R.K. Pandita, M.H. Porteus, D.J. Chen, J. Cote, T.K. Pandita, MOF and histone H4 acetylation at lysine 16 are critical for DNA damage response and double-strand break repair, *Mol. Cell Biol.* 30 (2010) 3582–3595.
- [28] L.R. Gurley, R.A. Walters, R.A. Tobey, The metabolism of histone fractions. Phosphorylation and synthesis of histones in late G1-arrest, *Arch. Biochem. Biophys.* 164 (1974) 469–477.
- [29] L.R. Gurley, R.A. Walters, R.A. Tobey, Cell cycle-specific changes in histone phosphorylation associated with cell proliferation and chromosome condensation, *J. Cell Biol.* 60 (1974) 356–364.
- [30] D. Bonenfant, H. Towbin, M. Coulot, P. Schindler, D.R. Mueller, J. van Oostrum, Analysis of dynamic changes in post-translational modifications of human histones during cell cycle by mass spectrometry, *Mol. Cell. Proteomics* 6 (2007) 1917–1932.
- [31] B.A. Garcia, C.M. Barber, S.B. Hake, C. Ptak, F.B. Turner, S.A. Busby, J. Shabanowitz, R.G. Moran, C.D. Allis, D.F. Hunt, Modifications of human histone H3 variants during mitosis, *Biochemistry* 44 (2005) 13202–13213.
- [32] J.A. Downs, S. Allard, O. Jobin-Robitaille, A. Javaheri, A. Auger, N. Bouchard, S.J. Kron, S.P. Jackson, J. Cote, Binding of chromatin-modifying activities to phosphorylated histone H2A at DNA damage sites, *Mol. Cell* 16 (2004) 979–990.
- [33] A.J. Morrison, J. Highland, N.J. Krogan, A. Arbel-Eden, J.F. Greenblatt, J.E. Haber, X. Shen, INO80 and gamma-H2AX interaction links ATP-dependent chromatin remodeling to DNA damage repair, *Cell* 119 (2004) 767–775.
- [34] R. Shroff, A. Arbel-Eden, D. Pilch, G. Ira, W.M. Bonner, J.H. Petrini, J.E. Haber, M. Lichten, Distribution and dynamics of chromatin modification induced by a defined DNA double-strand break, *Curr. Biol.* 14 (2004) 1703–1711.
- [35] J.S. Iacovoni, P. Caron, I. Lassadi, E. Nicolas, L. Massip, D. Trouche, G. Legube, High-resolution profiling of gammaH2AX around DNA double strand breaks in the mammalian genome, *EMBO J.* 29 (2010) 1446–1457.
- [36] E.P. Rogakou, C. Boon, C. Redon, W.M. Bonner, Megabase chromatin domains involved in DNA double-strand breaks in vivo, *J. Cell Biol.* 146 (1999) 905–916.
- [37] W.L. Cheung, F.B. Turner, T. Krishnamoorthy, B. Wolner, S.H. Ahn, M. Foley, J.A. Dorsey, C.L. Peterson, S.L. Berger, C.D. Allis, Phosphorylation of histone H4 serine 1 during DNA damage requires casein kinase II in *S. cerevisiae*, *Curr. Biol.* 15 (2005) 656–660.
- [38] R.T. Utley, N. Lacoste, O. Jobin-Robitaille, S. Allard, J. Cote, Regulation of NuA4 histone acetyltransferase activity in transcription and DNA repair by phosphorylation of histone H4, *Mol. Cell Biol.* 25 (2005) 8179–8190.
- [39] A.C. Harvey, S.P. Jackson, J.A. Downs, *Saccharomyces cerevisiae* histone H2A Ser122 facilitates DNA repair, *Genetics* 170 (2005) 543–553.
- [40] J.D. Moore, O. Yazgan, Y. Ataian, J.E. Krebs, Diverse roles for histone H2A modifications in DNA damage response pathways in yeast, *Genetics* 176 (2007) 15–25.
- [41] A. Sakaue-Sawano, K. Ohtawa, H. Hama, M. Kawano, M. Ogawa, A. Miyawaki, Tracing the silhouette of individual cells in S/G2/M phases with fluorescence, *Chem. Biol.* 15 (2008) 1243–1248.
- [42] E. Bartova, V. Foltankova, S. Legartova, P. Sehnalova, D.V. Sorokin, J. Suchankova, S. Kozubek, Coilin is rapidly recruited to UVA-induced DNA lesions and gamma-radiation affects localized movement of Cajal bodies, *Nucleus* 5 (2014) 460–468.
- [43] S. Legartova, A. Jugova, L. Stixova, S. Kozubek, M. Fojtova, Z. Zdrahal, G. Lochmanova, E. Bartova, Epigenetic aspects of HP1 exchange kinetics in apoptotic chromatin, *Biochimie* 95 (2013) 167–179.
- [44] G. Sustackova, S. Kozubek, L. Stixova, S. Legartova, P. Matula, D. Orlova, E. Bartova, Acetylation-dependent nuclear arrangement and recruitment of BMI1 protein to UV-damaged chromatin, *J. Cell. Physiol.* 227 (2012) 1838–1850.
- [45] L. Cincarova, G. Lochmanova, K. Novakova, P. Sultesova, H. Konecna, L. Fajkusova, J. Fajkus, Z. Zdrahal, A combined approach for the study of histone deacetylase inhibitors, *Mol. Biosyst.* 8 (2012) 2937–2945.
- [46] M.D. Plazas-Mayorca, B.M. Zee, N.L. Young, I.M. Fingerman, G. LeRoy, S.D. Briggs, B.A. Garcia, One-pot shotgun quantitative mass spectrometry characterization of histones, *J. Proteome Res.* 8 (2009) 5367–5374.
- [47] S. Sidoli, N.V. Bhanu, K.R. Karch, X. Wang, B.A. Garcia, Complete workflow for analysis of histone post-translational modifications using bottom-up mass spectrometry: from histone extraction to data analysis, *JoVE* (2016).
- [48] S. Brabencova, I. Ihnatova, D. Potesil, M. Fojtova, J. Fajkus, Z. Zdrahal, G. Lochmanova, Variations of histone modification patterns: contributions of inter-plant variability and technical factors, *Front. Plant Sci.* 8 (2017 Dec 7) 2084, <https://doi.org/10.3389/fpls.2017.02084>, eCollection 2017.
- [49] M.A. Dawson, A.J. Bannister, B. Gottgens, S.D. Foster, T. Bartke, A.R. Green, T. Kouzarides, JAK2 phosphorylates histone H3Y41 and excludes HP1 α from chromatin, *Nature* 461 (2009) 819–822.
- [50] L. Stixova, T. Hruskova, P. Sehnalova, S. Legartova, S. Svidenska, S. Kozubek, E. Bartova, Advanced microscopy techniques used for comparison of UVA- and gamma-irradiation-induced DNA damage in the cell nucleus and nucleolus, *Folia Biol.* 60 (Suppl 1) (2014) 76–84.
- [51] S. Legartova, J. Suchankova, J. Krejci, A. Kovarikova, E. Bartova, Advanced confocal microscopy techniques to study protein-protein interactions and

- kinetics at DNA lesions, *JoVE: JoVE* (2017).
- [52] A. Sillen, Y. Engelborghs, The correct use of "average" fluorescence parameters, *Photochem. Photobiol.* 67 (1998) 475–486.
- [53] Y. Yu, Y. Teng, H. Liu, S.H. Reed, R. Waters, UV irradiation stimulates histone acetylation and chromatin remodeling at a repressed yeast locus, *Proc. Natl. Acad. Sci. U. S. A.* 102 (2005) 8650–8655.
- [54] C. Hauser, B. Schuettengruber, S. Bartl, G. Lagger, C. Seiser, Activation of the mouse histone deacetylase 1 gene by cooperative histone phosphorylation and acetylation, *Mol. Cell Biol.* 22 (2002) 7820–7830.
- [55] S.J. Allison, J. Milner, Loss of p53 has site-specific effects on histone H3 modification, including serine 10 phosphorylation important for maintenance of ploidy, *Canc. Res.* 63 (2003) 6674–6679.
- [56] S. Banerjee S, G.R. Bennion, M.W. Goldberg, T.D. Allen, ATP dependent histone phosphorylation and nucleosome assembly in a human cell free extract, *Nucleic Acids Res.* 19 (1991) 5999–6006.